

Genus Topology and Cross-Correlation of BICEP2 and Planck 353 GHz B-Modes: Further Evidence Favoring Gravity Wave Detection

Wesley N. Colley^{1*} and J. Richard Gott, III^{2*}

¹University of Alabama in Huntsville Center for Modeling, Simulation and Analysis, Huntsville, AL 35899, USA

²Princeton University Department of Astrophysics Sciences, Princeton, NJ 08544, USA

Accepted 2014 December 01. Received 2014 November 25; in original form 2014 September 14

ABSTRACT

We have analyzed the genus topology of the BICEP2 B -modes and find them to be Gaussian random phase as expected if they have a cosmological origin. These BICEP2 B -modes can be produced by gravity waves in the early universe, but question has arisen as to whether these B -modes (for $50 < l < 120$) may instead be produced by foreground polarized dust emission. The dust emission at 150 GHz observed by BICEP2 should be less in magnitude but similar in structure to that at 353 GHz. We have therefore calculated and mapped the B -modes in the BICEP2 region from the publicly available Q and U 353 GHz preliminary Planck polarization maps. These have a genus curve that is different from that seen in the BICEP2 observations, with features at different locations from those in the BICEP2 map. The two maps show a positive correlation coefficient of $15.2\% \pm 3.9\%$ (1σ). This requires the amplitude of the Planck ($50 < l < 120$) dust modes to be low in the BICEP2 region, and the majority of the Planck 353 GHz signal in the BICEP2 region in these modes to be noise. We can explain the observed correlation coefficient of 15.2% with a BICEP2 gravity wave signal with an rms amplitude equal to 54% of the total BICEP2 rms amplitude. The gravity wave signal corresponds to a tensor-to-scalar ratio $r = 0.11 \pm 0.04$ (1σ). This is consistent with a gravity wave signal having been detected at a 2.5σ level. The Planck and BICEP2 teams have recently engaged in joint analysis of their combined data—it will be interesting to see if that collaboration reaches similar conclusions.

Key words:

cosmology: cosmic background radiation—cosmology: observations—cosmology: cosmological parameters—methods: statistical

1 INTRODUCTION

The BICEP2 team has announced discovery of B polarization modes on angular scales of 1° to 5° ($l = 40$ to $l = 200$) which are of an amplitude and angular scale that are too large to be due to gravitational lensing (BICEP2 Collaboration 2014). These B -modes are just in line with what would be expected from gravity waves from the early universe (Seljak & Zaldarriaga 1997, Kamionkowski et al. 1997). Their results suggest that if dust contamination is small (they have picked a region of the sky with very little foreground dust), the tensor-to-scalar ratio is $r = 0.2$ as compared with a value of $r = 0.13$ expected from simple single-field slow-

roll chaotic inflation (Linde 1983) with a simple quadratic potential $V(\phi) = (1/2)m^2\phi^2$ representing a simple massive scalar field (with mass m)—for possible implications for dark energy, see Slepian et al. 2014, Gott & Slepian 2011. The BICEP2 B -mode map is several σ in terms of signal-to-noise, and they find the same modes however they rotate their telescope and whether they consider the first or last half of their data. There thus seems little question that this signal is on the sky and not an instrumental effect. A simulation they present shows that the B -modes observed have significantly larger amplitude than would be expected from gravitational lensing. The main question seems to be whether the B -modes could instead be due entirely to B -modes produced by foreground dust. The BICEP2 team estimates that the dust contamination is low corresponding to a false value of $r = 0.04$ at most, and that their signal is produced by gravity waves

* E-mail: colleyw@uah.edu (WNC); jrg@astro.princeton.edu (JRG)

with $r > 0.16$. The BICEP2 region was chosen to be one of the least contaminated by dust in the entire sky. Mortonson, and Seljak (2014) and Flauger, Hill & Spergel (2014) argue that given the uncertainties of the amplitude of the dust polarization at the BICEP2 frequency of 150 GHz one cannot say conclusively at present whether the B -modes detected by BICEP2 are due to gravity waves or just polarized dust. All of these studies looked at the power spectrum of the B -modes. Flauger, Hill & Spergel (2014) in particular, fitting the B -modes power spectrum on the 1° to 5° scale, find that a model with $r = 0.2$ and no appreciable dust polarization (reduced $\chi^2 = 1.1$) is acceptable, as well as a model with $r = 0$ and dust B -modes (reduced $\chi^2 = 1.7$). They thus conclude that given the present uncertainty in the amplitude of the dust emission B -modes at 150 GHz one cannot say at present whether the BICEP2 B -modes are due to gravity waves or dust polarization. Those authors have digitized a publicly available Planck polarization map to compare with the BICEP2 map. We will similarly digitize and utilize this publicly available Planck polarization map in our study.

2 STUDY DESIGN

The main uncertainty seems to be the amplitude of the dust signal in the BICEP2 map. Therefore we designed a study to test between a gravity wave versus dust origin for the BICEP2 B -modes that does not depend on the amplitude of the dust signal at all.

We have previously used genus statistics to study the 3D topology of large scale structure and the 2D topology of hot and cold spots in the microwave background. The results of all these studies have been consistent with Gaussian random phase initial conditions demanded by inflation (Gott et al. 2007, Colley et al. 2003, Colley et al. 1996). In the cosmic microwave background our genus statistic is $g(\nu) = \text{number of hot spots} - \text{number of cold spots}$, where ν is the number of standard deviations above the mean temperature. For a Gaussian random phase distribution $g(\nu) = \nu \exp(-\nu^2/2)$.

We (Colley & Gott 2003) have found that the genus topology of the WMAP temperature field is in agreement with the Gaussian random phase model. Departures from a Gaussian random phase distribution can be quantified by the parameter f_{NL} invented by Komatsu & Spergel (2000). A perfect Gaussian random phase distribution would have $f_{NL} = 0$. The smallest detectable levels from the CMB would be of order 5. Standard slow-roll inflation (a simple field rolling down a hill) predicts values of f_{NL} of 10^{-2} to 10^{-1} (close to zero and undetectable with current data) according to calculations by Maldacena (2005) and others. For gravity waves Maldacena and Pimentel (2011) conclude that $f_{NL} \sim 1$, again essentially undetectable. Thus, standard inflation predicts values of f_{NL} near zero—consistent with a Gaussian random phase distribution. For comparison, the COBE results set 68% confidence limits of $-1500 < f_{NL} < 1500$. Using 2D genus topology on the WMAP data, we were able to improve these limits to $-101 < f_{NL} < 107$ at the 95% confidence level (Gott et al. 2007). The WMAP team found $-58 < f_{NL} < 134$ with an independent analysis (Spergel et al. 2007). All these ranges are consistent with f_{NL} near zero. The Planck satellite, drawing upon a much higher resolution map, and testing for random phases

with a different (bi-spectrum) method, has recently found $-3.1 < f_{NL} < 8.5$ (at 68% confidence) (Planck Collaboration 2013), again consistent with $f_{NL} = 0$ and the predictions of standard inflation. Gravity waves should thus produce Gaussian random phase fields to our limits of detection with 2D genus topology.

The differential operators used to calculate the B -modes when applied to a Gaussian random field, yield a Gaussian random field. This is particularly clear when one considers this in spherical harmonics where the operators applied to the Q and U maps are calculated by multiplying a_{lm} 's by factors involving l , but the Gaussian form of their amplitude distributions and their random phases are not altered. Therefore, if the B -modes from BICEP2 are cosmological, due to gravity waves in the early universe we expect their genus curves to be consistent with the Gaussian random phase formula. If that is observed it will favor gravity waves over dust polarization because dust polarization in a low dust region is not necessarily guaranteed to be Gaussian random phase, consisting of perhaps only a few polarizing sheets of dust in the line of sight. This phase of the study uses only the BICEP2 data with no reliance on Planck data at all.

In the second phase of the study, we will use the publicly available Planck data at 353 GHz (Stokes polarization parameters Q and U) to compute the B polarization modes. At this frequency, polarized B -mode emission is surely dominated by dust; so we will assume that any signal in the B polarization modes is due to dust. We will then compare the genus curve for the Planck 353 GHz map to that seen in the BICEP2 data. If they agree, that is evidence in favor of $r = 0$ and dust polarization only. In addition we will compare the 353 GHz B -mode map with the BICEP2 B -mode map. If the two agree with positive and negative (clockwise and counterclockwise swirls in polarization) regions at the same locations this would constitute a proof that the BICEP2 B -mode polarization was due to dust and not cosmological. It would falsify the claim that the particular B -modes seen in the BICEP2 map were due to gravity waves. We are making no specific assumption about the amplitude of the polarization at 150 GHz, just that the dust is in the same locations and that the polarization angles are similar at the two frequencies. If the B -modes from the dust are non-Gaussian random phase, all the better. We expect the B -modes from the dust to produce a complicated map, which we will compare directly to the B -modes in the BICEP2 data to look for coincidences. If all the features detected in the BICEP2 B -mode map are explained by features already found in the Planck dust dominated B -mode map the detection of gravity waves will be falsified.

The study is designed to go either way: supporting the detection of gravity waves if the BICEP2 B -mode map is Gaussian random phase and quite different from the Planck 353 GHz B -mode map, and refuting the detection if the BICEP2 and Planck 353 GHz B -mode maps are nearly identical.

Previous studies have considered the power spectrum of the B -modes. But this leaves out the other information in the maps. One of us (WNC), in his thesis produced two maps with identical power spectra, where one was Gaussian random phase and the other showed a Taco Bell logo (Colley 1998). The only difference was the non-random

phase nature of the second picture. The first picture looked like noise, and in the second one could see a blurry Taco Bell sign. The genus statistic easily distinguished between these two; the first fit the Gaussian random phase formula $g(\nu) = \nu \exp(-\nu^2/2)$, while the second just counted the particular cold spots for the letters and stylized bell in the logo over a wide range of ν , and was not in agreement with the random phase formula. Looking at the power spectrum alone is insufficient.

It is important whether the B -modes detected by BICEP2 show up in the Planck dust polarization B -mode maps or not. Note we are only considering the locations of the features not their amplitude. And we are only making use of the publicly available BICEP2 data and Planck data that were already utilized by the BICEP2 team and Flauger, Hill, and Spergel (2014). We are just using them in a different, and complimentary way.

3 USING THE BICEP2 MAPS

To create a usable version of the BICEP2 data, we first had to convert the figures from the PDF document (BICEP2 Collaboration 2014b) into usable data, showing the amplitude of the B -modes as a function of position on the sky. The PDF shows the E - and B -mode signals observed by BICEP and simulated E and B maps of expected backgrounds, chiefly gravitational lensing. First, we simply displayed the PDF such that each figure was at nearly the full resolution of the screen (a standard 1920×1080 HD display), and used a screen grabber to generate a PNG image. These maps present the major difficulty in that they are shown with black “headless” vector indicators of the polarization direction. To handle this, we created a custom Java program that first displays the trace of the color table (from the scale bar) on top of three two-dimensional histograms of pixel values in the map, where the axes of these histograms are the R and G levels, the G and B levels and the B and R levels in the RGB pixel data. What was quite apparent was that the majority of the pixel data indeed lay along the trace of the color table from the scale bar, but that there were also “echoes” of this trace at lower intensity for a much lower number of pixels. These turn out to be the pixels where there is anti-aliasing of the black headless vector segments. Fortunately, these echoes are sufficiently separated from the full intensity color table trace that one can readily identify which pixels have the full intensity, and which do not (in practice, for each pixel we found the minimum RGB distance from segments along the natural color table trace, and any with a minimum distance of greater than 4 was regarded to be corrupted by headless vector segment or its anti-aliasing pixels). For each excluded pixel, we searched to find the nearest 3 non-excluded pixels that geometrically enclosed the original pixel. This forms three triangles in the spaces (x, y, R) , (x, y, G) and (x, y, B) . Treating each triangle as a plane, we interpolated to the original pixel location and used that interpolated value to replace the original excluded pixel value. The natural outputs are PNG maps on which the headless vectors have been removed. However, because we have referenced to the the scale bar color table in this process, we can also output each map’s values in physical units.

We now have physical-unit maps for each of the four

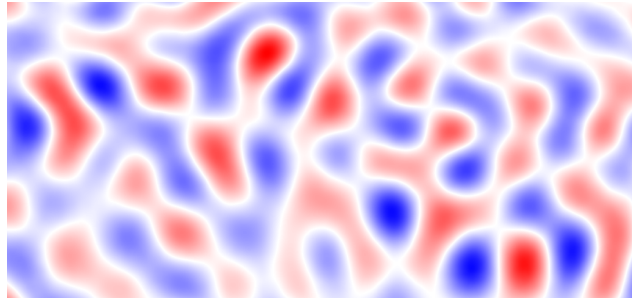


Figure 1. BICEP2 B -modes in Mercator projection in the region $|\text{RA}| \leq 30^\circ$, $-65^\circ \leq \text{Dec} \leq -50^\circ$. The stretch is from $-0.271\mu\text{K}$ (blue) to $0.271\mu\text{K}$ (red).

original map images (E , B , simulated E and simulated B). For analysis, we smooth these maps with a Gaussian kernel with $\sigma = 5$ pixels. This not only smooths over the blocky appearance of the original BICEP2 maps, but also smooths over the generally minor artifacts arising from the headless vector removal process.

The next problem is that of the sensitivity, which is non-uniform across the maps. Fortunately, the BICEP2 Collaboration (2014c) has provided a map over their sensitivity in Fig. 24. We used this sensitivity map to normalize the BICEP B -mode data, and cut our analysis region to $|\text{RA}| \leq 30^\circ$, $-65^\circ \leq \text{Dec} \leq -50^\circ$, inside of which the lowest weight was roughly 0.3. Finally, we projected this flattened map into Mercator (Fig. 1) and Lambert equal-area cylindrical projections. Using two different projections was necessary—for statistical measurements on the map, we chose the equal-area projection, but for the genus, we chose the Mercator projection. The conformal Mercator projection preserves angles on the sphere locally. This ensures that the density contour surfaces meet the survey boundary at the correct angles. The color scheme in Fig. 1 is one we used in Gott et al. (2007). White is a B -mode of zero. Red ink indicates positive B -mode with the amount of red ink per pixel proportional to the value of the positive B -mode at that location. Blue ink indicates negative B -mode with the amount of blue ink per pixel proportional to the amount of negative B -mode at that location.

4 DEVELOPMENT OF THE DUST B -mode MAP

The Planck team (Boulanger 2014) has provided the I , Q and U maps of dust polarization. The Q and U maps are presented in a Mollweide projection, with color table scales given below each. The first task is, therefore, to convert the color table images back to physical units. Our process is quite similar to that described for the BICEP2 map above, except without the pesky headless vectors to clean up. We first displayed the PDF and did a simple screen grab at a high zoom level, to convert the PDF data to standard PNG pixel data. In IDL, at each pixel location, we found in RGB vector space the three RGB values from the color scale that minimized the distance between themselves and the pixel’s RGB values. We then fit a quadratic function to the squared RGB distances. Minimizing the quadratic gave us an interpolated locus on the color scale, which we trans-

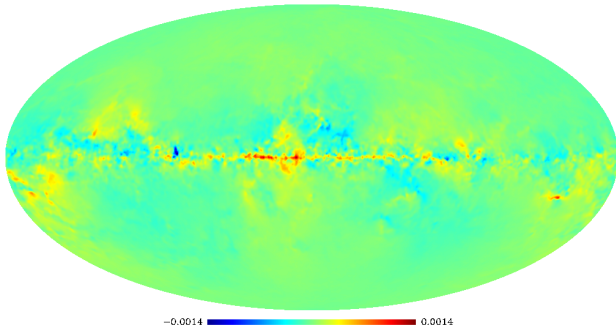


Figure 2. All-sky map of the B -modes from the publicly available Planck Q and U maps we have digitized and where we have computed the B polarization modes. The units in the scale measure fluctuations in brightness temperature (K).

lated to temperature using the scale’s stated graduation. The result was a Mollweide projection of both the Q and U polarization maps in physical units, namely Kelvins. But to compare with the BICEP2 B -mode map, we obviously needed to convert the Q and U to B .

For the B -mode analysis, we used the HEALPix library (e.g., Górski et al. 2005). Using the IDL interface, we iterated over all the HEALPix pixels at a resolution level of $n_{\text{side}} = 512$, and projected them back to the Mollweide map to find the location in our Q and U Mollweide maps (we simply used bilinear interpolation to estimate the temperature value at a particular HEALPix pixel location). We then had a HEALPix map for the Q and U dust maps.

Computing the B -mode values was straight-forward with the standard modules inside the HEALPix library; the internal mathematical techniques are described by Guzik et al. (2000). Our approach was to develop a C++ program which loaded the HEALPix Q and U maps, and then called the `map2alm_spin` routine, whose documentation (Hivon 2010) explains that by calling the routine with a spin argument of 2, it takes as input the Q and U maps, and outputs the spin zero a_{lm} values for the E - and B -modes associated with the Q and U polarizations. From there, it is just a matter of using the usual (spin zero) `alm2map` routine to convert a_{lm} values into a sky map of the B -modes of the dust, as observed by Planck. Fig. 2 shows the result of this process. Fig. 5 shows the dust map in just the BICEP2 region (as a Mercator projection).

The Planck B -mode map described above (Fig. 5) clearly looks nothing like the BICEP2 B -mode map. However, the BICEP2 team conducted some data processing that one must mimic in order to conduct statistical analyses. In particular, the BICEP2 map only shows modes from $50 < l < 120$ and has been “desplined” as we shall describe. We will use 5 somewhat different techniques with various degrees of complexity for achieving this.

First, let us consider the effects of filtering the l modes to $50 < l < 120$. Fig. 3 shows the filtered Planck 353 GHz B -modes in the BICEP2 region. Note the striations. If we consider the whole sky for the same map (Fig. 4), we see that the pattern of striations extends to larger scales in the low B -mode regions. The filtering gives the map a uniformly choppy look because we are only looking at a small range

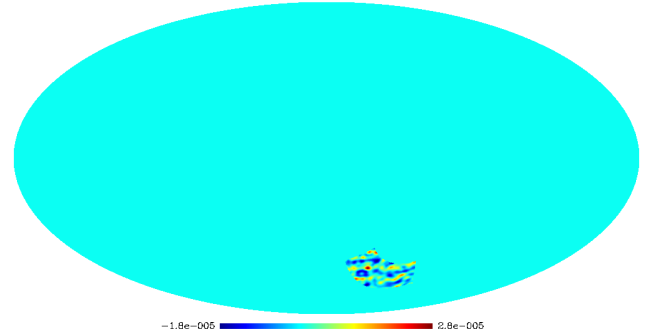


Figure 3. Planck 353 GHz B -modes in the BICEP2 analysis region, using $50 < l < 120$ B (in K). Note the striations.

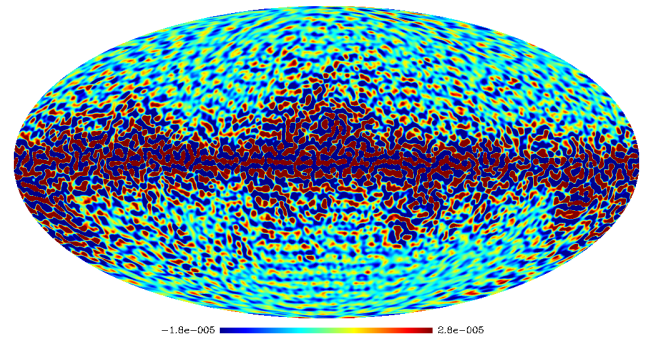


Figure 4. Planck 353 GHz B -modes for the full sky, using $50 < l < 120$ B (in K), stretched as in Fig. 3. This stretch saturates high values near the plane as red, and low values as blue. Notice the uniform appearance of the multicolor (blue to green to red) regions, suggesting one is hitting instrumental noise and/or systematic effects. Note that there are no regions with smaller fluctuations—no pure green regions.

of modes. The color scale saturates at pure red or pure blue beyond the extremes in B -mode amplitude seen in the BICEP2 region. Fig. 3 shows just the BICEP2 region. It has a rainbow color scale for the amplitude of the B -mode with the red end of the spectrum positive and the blue end of the spectrum negative. Fig. 4 shows this extended to the whole sky with the map saturating at pure red or pure blue if it exceeds the magnitude of the B -mode seen anywhere in the BICEP2 region. The modes $50 < l < 120$ are just the ones where the gravity waves might exceed the dust in BICEP2. At smaller scales gravitational lensing would dominate, and at larger scales dust would dominate because of its flatter power spectrum. The striations appear to cover the whole map running in different directions. In the galactic plane the striations have stripes parallel to the plane, but at high latitudes they run in different directions. Some regions look more checkerboard like. The regions of highest $50 < l < 120$ B -mode amplitude (pure red or pure blue) follow the well-known structures in the galaxy, where the amplitude of dust emission is greatest. But the regions in rainbow colors like the BICEP2 region all look surprisingly similar, suggesting we are looking at mostly instrumental and systematic noise. The striations appear to be due to ringing in these modes due to fitting the structures in high intensity regions.

The unsaturated regions (like BICEP2) look surpris-

ingly uniform, they all have striations that look surprisingly similar. Once one hits the noise level, full of ringing modes, the sky looks relatively uniform. There are no areas of lower signal (no large patches of pure green in the map). This suggests a large amount of noise dominating the dust signal. We have developed five different mapping techniques to address these issues and produce the best ($50 < l < 120$) 353 GHz B -mode map in the BICEP2 region, with the least contamination from modes ringing off high intensity regions elsewhere in the sky. The BICEP2 team only had data in their survey region and would not be influenced by modes ringing off structures elsewhere.

The first map for analysis, Map I, used the most straight-forward means of construction of our 5 maps. As with all maps, we took the a_{lm} modes from the B map produced by HEALPix analysis, and use only those with $50 < l < 120$, to produce the output map. We further eliminated the $m = 0$ modes (in Galactic coordinates), to dampen some of the ringing effects from the Galactic plane discussed above. Following the BICEP2 team’s techniques, we also corrected the map by subtracting the best-fit horizontal (in right ascension) cubic spline, with two intervals joined in the middle of the map (which we shall call “desplining”). We use this in all our maps.

For Map II, we used a similar analysis procedure. However, we were more aggressive in addressing the ringing in the Fourier modes from the plane of the Galaxy. Thus, we removed the plane by excising the 20% of the sky centered on the Galactic Equator, and smoothly interpolating across the region with a cosine-filter. This technique was quite successful in reducing the impact of the ringing, which can be seen by the fact that the r.m.s. of the pixel values (away from zero) is reduced from $4.97\mu\text{K}$ to $3.31\mu\text{K}$ in the region to be compared with BICEP2. The removal of the plane was sufficient to obviate the need to remove the $m = 0$ modes.

For Map III, we reduced the ringing even further. To do this, we selected a mask the size of the entire BICEP2 region. However, in this case, we could more closely mimic the BICEP2 analysis by displining first, before sending the map to HEALPix. This technique continued to reduce the ringing noise level, leaving a standard deviation from zero of $3.12\mu\text{K}$. Note that for these last three maps, we used the Fortran 90 HEALPix implementation, which facilitates use of masks. This map is shown in Fig. 6.

For Map IV, we took our displined map from Map III, but applied the BICEP2 sensitivity map as the mask during the HEALPix analysis. On the back end we corrected for this by dividing back off by the mask to flatten the image, just as we did for the actual BICEP2 data. This gives a standard deviation from zero of $2.96\mu\text{K}$. We show this map in Fig. 7.

For Map V, we did the most aggressive masking. We took our displined map from Map III, and masked down to just the region of analysis ($|\text{RA}| \leq 30^\circ$, $-65^\circ \leq \text{Dec} \leq -50^\circ$). This “what-you-see-is-what-you-get” or “wysiwyg” map has no influence from fitting the sky beyond the region we will actually analyze statistically. This gives a standard deviation from zero of $3.03\mu\text{K}$. We regard this map to be the “cleanest” in the sense that there should be minimum contamination from any other region of the sky.

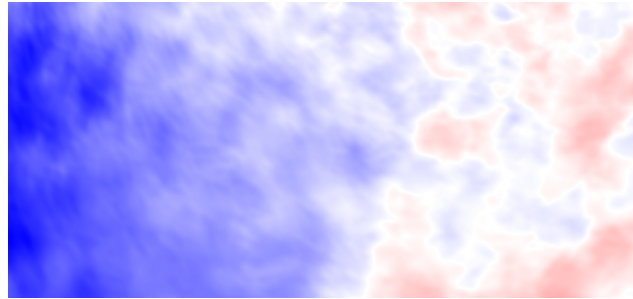


Figure 5. Planck 353 GHz polarization B -modes in Mercator projection in the region $|\text{RA}| \leq 30^\circ$, $-65^\circ \leq \text{Dec} \leq -50^\circ$. The stretch is from $-66.7\mu\text{K}$ (blue) to $66.7\mu\text{K}$ (red).

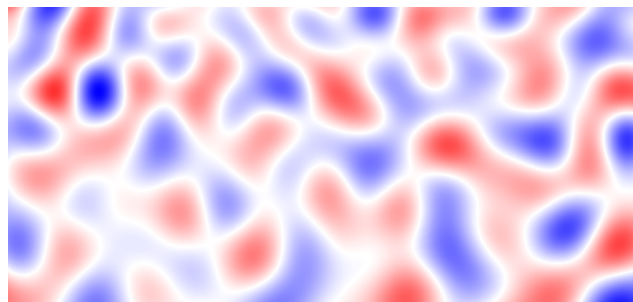


Figure 6. Map III: The Planck 353 GHz polarization B -modes in Mercator projection in the region $|\text{RA}| \leq 30^\circ$, $-65^\circ \leq \text{Dec} \leq -50^\circ$. The map has been constructed by using only the modes $50 < a_{lm} < 120$ to match the BICEP2 data process. The stretch is from $-11.5\mu\text{K}$ (blue) to $11.5\mu\text{K}$ (red). During construction of the B -mode map, a “large” mask the size of the entire BICEP2 region was used.

5 COMPUTING THE GENUS

The properties of the genus are well-known in three dimensions (3D) (Gott et al. 1986, Hamilton et al. 1986, Gott et al. 1987), but require some explanation in the two-dimensional (2D) case (Melott et al. 1989), particularly in the case of the sphere (Coles & Plionis 1991, Gott et al. 1990).

We can rigorously define the 2D genus on a spherical surface (e.g., Colley et al. 2003). The 2D genus is defined to be equal to minus the 3D genus of solid objects formed by bestowing the regions above a threshold with a small, but

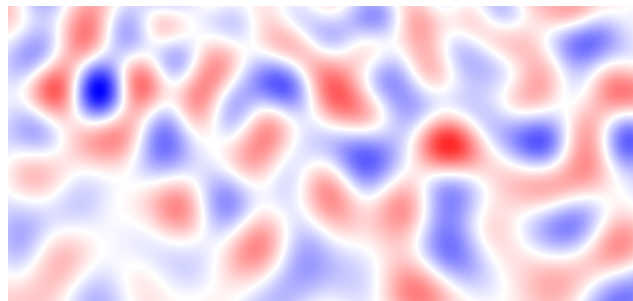


Figure 7. Map IV: As with Map III (Fig. 6), except that the mask used is the BICEP2 sensitivity map itself. This better approximates the apodization process BICEP2 used to reduce the number of ambiguous modes. Note that there is very little difference between Map III and Map IV.

finite radial extent. Imagine using lead paint to paint the hot regions onto the surface of a balloon, and after letting the paint dry, bursting the balloon to obtain solid, curved lead shapes that would have a certain 3D genus. Take the minus of this number and that will be g_{2D} , as we will define it.

One hot spot in the north polar region would have a 2D genus of +1 (one hot spot), because the hot spot cap is one isolated region. Suppose the hot region covered all of the sphere except for a cold spot in the south polar region. The genus would still be +1, because this would look like a sugar bowl without any handles, which is also one isolated region in 3D. The topology in each case is identical since one can be deformed into the other. The genus on a plane is determined by the local turning that a truck would do driving around the temperature contour surface. Circling a hot spot on a plane would require a total turning of 2π . The Gaussian random phase formula measures this local turning. Circling a hot spot on the sphere involves a total turning of $2\pi - 4\pi f$, where f is the fraction of the sphere in the hot spot (because the deficit produced by parallel transport on the sphere is equal to the enclosed area). Dividing by 2π , we may define the effective genus:

$$g_{2D,eff} = g_{2D} - 2f, \quad (1)$$

where f is the fraction of the area of the sphere in the hot spots. For a Gaussian random phase field on the sphere

$$g_{2D,eff} \propto \nu \exp(-\nu^2/2), \quad (2)$$

because the Gaussian random phase field behaves locally on the sphere just as it does on the plane to produce this particular contribution to the turning integral. The Mercator projection we have chosen preserves the turning, and thus the genus. Therefore, in comparing our genus curves to the random phase formula, we will use $g_{2D,eff}$, as defined rigorously above (cf., Colley et al. 2003).

The BICEP2 analysis region is a fairly thin strip of the southern sky within a fairly narrow range in declination ($-30^\circ \leq RA \leq 30^\circ$, $-65^\circ \leq Dec \leq -50^\circ$), which particularly lends itself to the Mercator projection (in celestial coordinates) shown in in Fig 1. To compute the genus we proceed with our normal two-dimensional genus calculations, using methods very similar to those of CONTOUR2D (Melott et al. 1989). Fig. 8 shows the 2D genus for the BICEP2 data, for a large number of ν values. The jaggedness of the genus trace conveys a sense of the error in the genus computation process. In practice, formal error bars are difficult to estimate, because the genus at nearby values is correlated (the same structures appear at similar thresholds). Gott et al. (2007) (among others) have demonstrated elaborate techniques for estimating χ^2 errors by using a large number of simulations to create a reliable covariance matrix that accommodates these correlations, but this is somewhat beyond our scope here. As a check, we did divide the region into four quadrants so that we could estimate errorbars and found that the genus matches the theoretical curve at (1σ) essentially across the board (better than expected for independent variates because of the correlations). Overall, the fit between the BICEP2 genus and the Gaussian random phase curve is excellent. The BICEP2 data pass this test.

Fig. 9 and Fig. 10 provide the genus curves for the dust maps, with all a'_{lm} s and with only the $50 < l < 120$ a'_{lm} s, re-

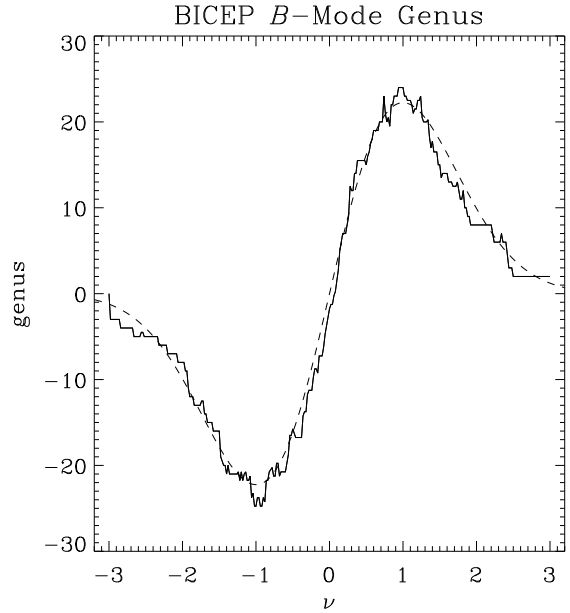


Figure 8. 2D genus for the BICEP2 data. Overplotted is the theoretical Gaussian random phase genus curve, where only the amplitude has been fit. The best-fit amplitude is 22.2 at $|\nu| = 1$.

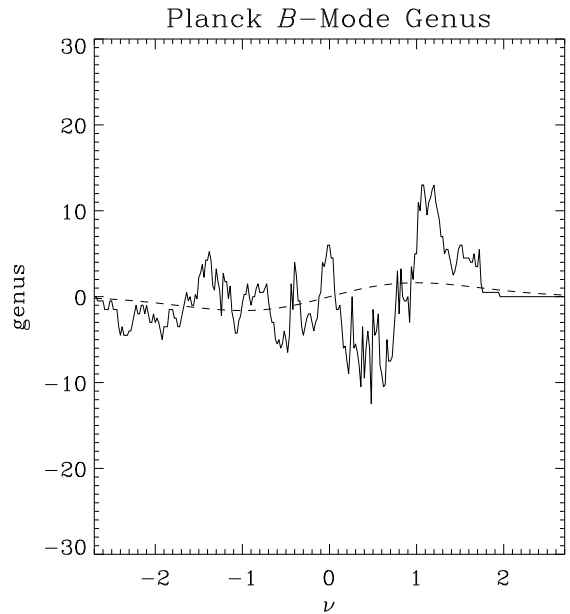


Figure 9. 2D genus for the Planck 353 GHz B -modes. Overplotted is the theoretical Gaussian random phase genus curve, where only the amplitude has been fit. The best-fit amplitude is 1.62 at $|\nu| = 1$.

spectively. Not surprisingly, for the full a_{lm} dust map, which looks nothing like a Gaussian random phase field, the genus curve looks nothing like the Gaussian random phase theoretical curve. However, the genus curve for the truncated a_{lm} map agrees very well with the Gaussian random phase theoretical curve, although at lower amplitude than seen in the BICEP2 genus curve.

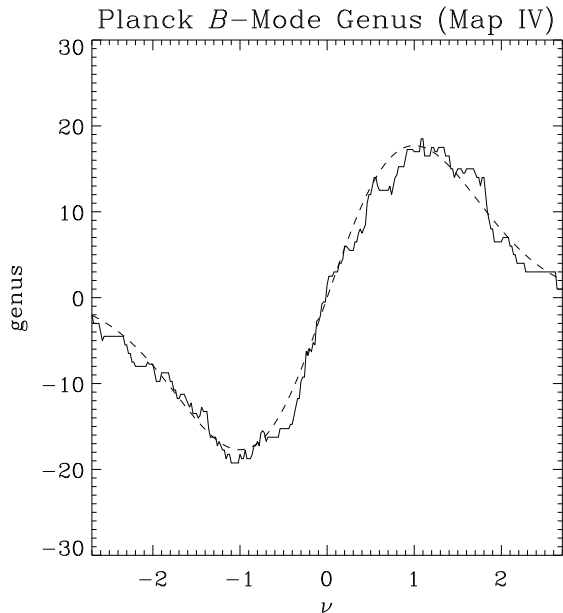


Figure 10. 2D genus for the Planck 353 GHz B -modes from our Map IV (see Fig. 7), which has been “desplined” in the BICEP2 region and masked to just the analysis region of $|\text{RA}| \leq 30^\circ$, $-65^\circ \leq \text{Dec} \leq -50^\circ$, and filtered to use only the $50 < a_{lm} < 120$ modes. Overplotted is the theoretical Gaussian random phase genus curve, where only the amplitude has been fit. The best-fit amplitude is 17.7 at $|\nu| = 1$.

One supposes the BICEP2 team wanted to show a map that would show just the modes where the gravity wave modes were most prominent. The BICEP2 team filtered out the low l modes to avoid confusion with the B -modes from gravitational lensing, and presumably filtered out the low l modes to avoid confusion with dust. This is because the power spectrum in the dust B -modes is very flat. For dust $l(l+1)C_l/2\pi \sim l^{-0.4}$. The flat nature of the power-spectrum for the dust is shown in Flauger, Hill & Spergel (2014). On the other hand, for the B -modes expected from gravity waves over the range $10 < l < 80$ have $C_l \sim \text{const}$, so that $l(l+1)C_l/2\pi \sim l^2$. (For $l > 100$ the gravity wave B -mode spectrum begins to fall and crosses below the gravitational lensing power at $l \approx 150$.) The gravity wave B -mode power spectrum over the range $10 < l < 100$ has less power at large scales than the dust B -modes and therefore by our genus formula a larger amplitude genus curve; the genus amplitude is proportional to $\langle k^2 \rangle$ integrated over the smoothed power spectrum (Melott et al. 1989). The BICEP2 map has a choppier distribution than does the Planck map. When Flauger, Hill, and Spergel (2014) measure the χ^2 for the gravity wave fit to the BICEP2 B -mode power spectrum data ($50 < l < 175$) they obtain 1.1, the dust fit is worse at 1.7 but not horrible. The BICEP2 data does follow closely the expected power spectrum for the gravity wave modes including the fact that $l(l+1)C_l$ in the modes at $l = 50$ is lower than at $l = 75$ as expected from gravity waves rather than higher as would be expected for dust B -modes only. The errors in the individual l modes are enough to make the flatter dust distribution not look all that bad, its amplitude can be fit to give the right level and then it is simply

a bit too high at the low l end and a bit low at the high l end. This is particularly true when one is also looking at the bump at the high l end where the gravity wave signal is flatter as well.

The amplitude of the genus curve can be very useful in checking the power spectrum of the cosmological model as has been shown by Park & Kim (2010) and Gott et al. (2009) for 3D topology. The fact that Flauger, Hill, and Spergel get a better fit for the steep gravity wave power spectrum than for the flatter dust spectrum, means that the filtered map that BICEP2 has is in agreement with the number of structures expected from the steep gravity wave spectrum. This is shown by the fact that the BICEP2 team has also included a simulation with B -modes produced by gravitational lensing only. The power spectrum from gravitational lensing over the range $10 < l < 100$ also has $C_l \sim \text{const}$ so that $l(l+1)C_l/2\pi \sim l^2$, it just has an amplitude that is too low to explain the BICEP2 data as they demonstrate. The gravitational lensing map BICEP2 shows for comparison has a similar number of structures, and a similar amplitude of the genus (it just has lower contrast.) Since the dust spectrum is flatter (and by the way is a poorer fit to the power spectrum) it should predict fewer structures than BICEP2 observes. The genus curve amplitude just provides a more dramatic illustration of this poorer fit.

The BICEP2 B genus curve shows a maximum of 22 red spots and 22 blue spots. The identically filtered Planck map showed only a maximum of 18 red spots and 18 blue spots (Fig. 10). That is consistent with a flatter power spectrum.

For a Gaussian random phase field, one also expects a Gaussian histogram. To calculate this we constructed maps using the Lambert equal area cylindrical projection (not shown), rather than the Mercator projection; this histogram for the BICEP2 B -modes is shown in Fig. 11. The Gaussian with $\mu \approx \bar{x}$ and $\sigma \approx s$ is shown on top of the histogram. As with the genus, the fit is excellent. This distribution is consistent with the Gaussian Random phase distribution expected from a cosmological origin due to gravity waves from inflation. We also show the histograms for the Planck maps, and as one might expect from Figs. 5, 6 and 7, the full a_{lm} map shows a highly non-Gaussian distribution (Fig. 12), while the truncated a_{lm} map shows a distribution very much consistent with a Gaussian (Fig. 13). As such, the BICEP2-like processing of the data appears to mask many non-Gaussianities in the dust-dominated Planck map. Kamionkowski & Kovetz (2014) have suggested using the hexadecapolar departure from isotropy to reveal the level of non-Gaussianity in the B -mode data introduced by foregrounds, but conclude the current signal-to-noise is insufficient for conclusive results.

6 DISCUSSION

If $r = 0$ and all the B -modes seen in the BICEP2 map are produced by dust, and Planck is detecting dust modes with ($50 < l < 120$) at high signal-to-noise then we would expect the two maps (Fig. 1 and Fig. 7) to have the same number of structures in the same locations. Visual inspection confirms the genus result that there are indeed fewer structures in the Planck map. If Planck is detecting the dust modes this suggests that a number structures in the BICEP2 map must

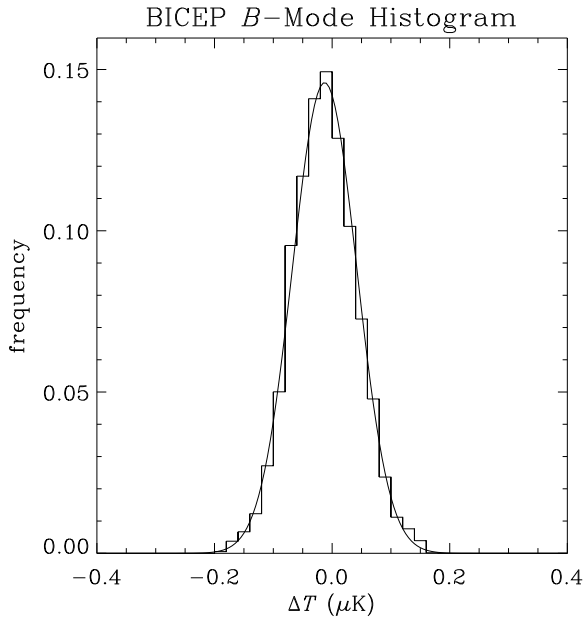


Figure 11. Histogram from an equal-area projection of the BICEP2 B -mode data. Overplotted is the normal curve associated with a simple computation of \bar{x} and s as estimators of the mean and standard deviation.

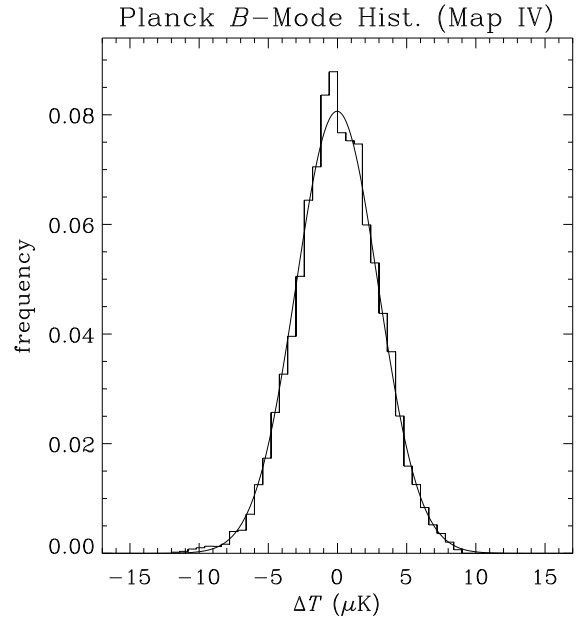


Figure 13. Histogram from an equal-area projection of Planck 353 GHz B -modes, computed after “despinning” in right ascension; only $50 < a_{lm} < 120$ modes are included (Map IV). Overplotted is the normal curve associated with a simple computation of \bar{x} and s as estimators of the mean and standard deviation.

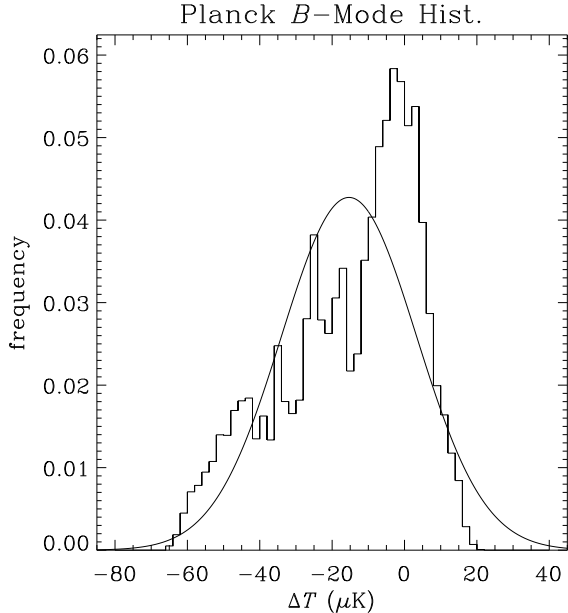


Figure 12. Histogram from an equal-area projection of Planck 353 GHz B -modes. Overplotted is the normal curve associated with a simple computation of \bar{x} and s as estimators of the mean and standard deviation.

be due to gravity waves. The 353 GHz map itself, of course, contains more information than contained in the power spectrum or the histogram or genus curve. We can ask for the correlation coefficient between the two maps. It is 15.2% (average for Maps I–V) showing that the location of the structures are mostly uncorrelated—as is apparent from a

visual inspection. The B -modes that BICEP2 is seeing are not the ones we are seeing in the Planck 353 GHz map.

The B -modes in BICEP2 are of too large an amplitude to be produced by gravitational lensing, as shown by a simulation which includes a standard flat lambda model and gravitational lensing only (BICEP2 Collaboration 2014a). The B -modes due to gravity waves also have $l(l+1)C_l/4\pi \sim l^2$ at low l but are of lower amplitude. This simulated map has a similar number of structures (consistent with what we would expect from the genus statistic), but its amplitude is too small to fit the BICEP2 data. This aspect of their study has not been questioned. In addition BICEP2 at smaller scales sees the gravitational lensing B -modes. The gravity wave modes kick in for $l < 100$ with higher amplitude in the B -mode power spectra, over and above the gravitational lensing B -modes. So it seems clear that BICEP2 is not seeing just gravitational lensing.

At this point we should mention another way to produce B -modes—Faraday Rotation—in order to immediately rule it out. Imagine that one has a pure E -mode with polarization directions that radially point away from a center. Faraday rotate all these polarization directions by 45° and you have produced a pure B -mode with a pinwheel pattern. The maximum amplitude of the E -mode detected by BICEP2 at $50 < l < 120$ is $\sim 1.7\mu\text{K}$ while the maximum amplitude of the B -mode is $\sim 0.3\mu\text{K}$. To produce this much B -mode from an E -mode would require a Faraday rotation of $\theta \sim \tan^{-1}[(0.3/\sqrt{2})/(1.7 + 0.3/\sqrt{2})] \sim 6.3^\circ$. Now the galactic foreground Faraday rotation in the BICEP2 region is fairly uniform at about $100\text{rad} \cdot \text{m}^{-2}\lambda^2$ (Opperman et al. 2011). At 150 GHz, $\lambda = 0.002\text{m}$, so the Faraday rotation is 0.0004 rad, far less than the required 0.1 radian. The additional Faraday rotation seen in quasars amounts to only an

additional $\pm 50 \text{rad} \cdot m^{-2} \lambda^2$ due to intervening clouds. Faraday rotation near recombination also is implausible since the wavelengths are shorter by a factor of 1000 than which lowers the Faraday rotation by a factor of a million. In any case, if Faraday rotation were responsible for the B -modes the B -mode and the E -modes in the BICEP2 map would be at identical locations—this is not the case. The E - and B -modes are at different locations in the BICEP2 maps. Thus, Faraday rotation can be ruled out as the source of the BICEP2 B -modes.

Flauger, Hill and Spergel (2014) have stated that the polarized B -mode amplitude is sufficiently uncertain that the results are either consistent with a B -mode signal from BICEP2 due to $r = 0.2$ and gravity waves or $r = 0$ and due to dust. We have not depended on the amplitude at all but have only gone on the structure of the 353 GHz modes, which do not match the visual appearance nor the amplitude of the genus curve in the BICEP2 data. If the structures seen in the BICEP2 map could readily identified with structures in the 353 GHz Planck map this would be a smoking gun implicating the dust. This is definitely not seen.

6.1 Amplitude Considerations

Now let us look at the amplitude for the first time. Our histogram shows the amplitude of the B -modes amplitude in the (spline subtracted) filtered $50 < l < 120$ BICEP2 map to be $0.0838 \mu\text{K}$ (1σ) at 150 GHz. The histogram of the B -mode amplitudes in the 353 GHz Map IV from Planck which we have constructed from their Q and U maps show the (spline subtracted) filtered $50 < l < 120$ B -mode amplitude to be $2.96 \mu\text{K}$, again in brightness temperature.

We have measured the power spectrum of our whole sky B -mode dust map at 353 GHz; it follows the simple power law form found by Planck and is at a higher amplitude than their 80% of the sky map which avoids the galactic plane. To compare with that 80% map, we have cleaned the Planck map of the 20% of the sky that includes the plane and we get the same amplitude power spectrum that the Planck team reports (Boulanger et al. 2014). This makes it clear that the scale in the Planck Q and U maps is in units of K in brightness temperature, which is what we have adopted.

The Planck collaboration estimates that the dust B -mode power spectrum should be lowered by a factor of 25.8^2 at 143 GHz relative to that at 353 GHz. We have taken this value from a power spectrum estimate for 143 GHz they have made publicly available. That implies they expect the amplitude of the dust signal at 143 GHz relative to 353 GHz to be lower by a factor of 25.8. If dust emission goes as $I_\nu \sim \nu^\gamma$ over that frequency range and the polarization fraction stays constant between 143 GHz and 353 GHz, then the amplitude of the dust map at 143 GHz should be lower (in brightness temperature) than that in the 353 GHz map by a factor of

$$\frac{e^{143/56.8}}{e^{353/56.8}} \left[\frac{e^{353/56.8} - 1}{e^{143/56.8} - 1} \right]^2 \left[\frac{353}{143} \right]^{\gamma-4} = 25.8, \quad (3)$$

where for the microwave background, $h\nu = kT$ at 56.8 GHz. This implies a value of $\gamma = 3.324$ over the frequency range from 143 GHz to 353 GHz which is plausible. If we use that value we can calculate using the same formula the lowering we expect from 353 GHz to 150 GHz. We find a factor of

23.1, (quite reasonable since we are moving over a slightly smaller frequency range).

Probably the best estimate of this factor is from the recent Planck data (Planck Collaboration 2014a) on polarization as a function of frequency. They estimate that the polarized dust emission $I_\nu \sim \nu^{3+\beta} / [e^{h\nu/kT_D} - 1]$, where $\beta = 1.65$, and $T_D = 19.8\text{K}$ for high latitude dust. (Thus $h\nu/kT_D = \nu/413.5\text{GHz}$.) This includes the fact that the polarized fraction is slightly lower at 150 GHz than at 353 GHz. This is consistent with Draine and Hensley's (2013) treatment of ferromagnetic nanoparticles in interstellar dust. For inclusions, magnetic dipole emission is expected to be polarized orthogonally relative to the normal electric dipole radiation. This can explain a somewhat smaller polarization fraction at 150 GHz than at 353 GHz. The factor β is derived empirically by the Planck team. We find that for polarized emission

$$I_{353}/I_{150} = \left(\frac{353}{150} \right)^{4.65} \frac{e^{150/413.5} - 1}{e^{353/413.5} - 1} = 17.35. \quad (4)$$

Converting fluctuations in intensity to fluctuations in brightness temperature in the CMB using

$$dI = d \left[\frac{2\pi h\nu^3 c^{-2}}{e^{h\nu/kT} - 1} \right] = \frac{2\pi h\nu^3 c^{-2} e^{h\nu/kT}}{(e^{h\nu/kT} - 1)^2} (h\nu/kT^2) dT, \quad (5)$$

where $h\nu/kT = h\nu/(k \cdot 2.72\text{K}) = \nu/56.8\text{GHz}$, we find for polarized dust emission:

$$\frac{\Delta T_{353}}{\Delta T_{150}} = 17.35 \cdot \left[\frac{353}{150} \right]^{-4} \left[\frac{e^{150/56.8}}{e^{353/56.8}} \right] \left[\frac{e^{353/56.8} - 1}{e^{150/56.8} - 1} \right]^2 = 21.3,$$

which we will adopt.

This is quite similar to the original Planck derived estimate of 23.1 mentioned above, but this is more accurate, based on later and more complete data.

As we shall see later, the BICEP2 map and the Planck 353 GHz map have a correlation of only 15.2%. If we attributed that to supposing that the dust signal at 150 GHz was 15.2% of the total BICEP2 signal which we would believe was primarily due to gravity waves, we would be left with the untenable conclusion that the polarized dust emission in this particular region must fall off as we go from 353 GHz to 150 GHz by a factor of 11.1 *more* than we expect (i.e., a factor of $[0.142 \mu\text{K}/0.0838 \mu\text{K}]/0.152$). Dust can have different polarization fractions at different frequencies due to grain properties, but this much lowering seems implausible. In addition the Planck data shows evidence for a small change in polarization fraction from 150 GHz to 353 GHz and this has already been included. So if the Planck 353 GHz map were a pure dust signal with little noise contamination, the scenario that the dust signal at 150 GHz was sub-dominant would not work.

Can the fallen-off dust signal be equal to the BICEP2 signal? Against that simple interpretation (that the BICEP2 signal is a pure high signal-to-noise dust signal which can be seen in the 353 GHz map) is the fact that the observed BICEP2 pattern does not match the Planck 353 GHz pattern.

By the way, we expect the BICEP2 $50 < l < 120$ B mode signal if it is cosmological and due to gravity waves, to have the same amplitude in brightness temperature at 353 GHz as it does at 150 GHz: $0.0838 \mu\text{K}$ (1σ). Thus, under no circumstance do we expect the gravity wave signal to

significantly pollute the Planck signal of $2.96\mu\text{K}$ (1σ) at 353 GHz.

By contrast we may expect the dust emission at 353 GHz to pollute the BICEP2 signal at 150 GHz to some extent. Indeed this seems to be the case. We do find a correlation coefficient of 0.181 between the filtered BICEP2 map and the similarly filtered 353 GHz map from Planck (Map IV, shown in Fig. 7). This suggests that the dust is peeking through in both maps (the correlation is positive).

We now consider the uncertainties associated with the correlation coefficients C_{PB} . To this end, for each map, we computed the correlations between not only the dust map and the BICEP2 map, but also between the vertically and/or horizontally flipped dust map and the BICEP2 map. This gave us 3 fairly independent measures for the level of correlation one might expect if there were no dust contamination. We went one step further, which was to conduct exactly the same experiment using maps constructed from the sky at the opposite galactic longitude, where there appears to be very similar structure in Fig. 4 to that in the BICEP2 region. Each of the four available flips should be uncorrelated with the BICEP2 map. This gives us 7 presumably uncorrelated maps to evaluate for each of our map methods. With our 5 methods, we now have 35 values from which to form an estimate of the typical variation in the correlation. The standard deviation for all 35 is 0.039. This is consistent with the variation seen in the last 4 maps (Maps II – V, where the impact of the plane has been reduced one way or the other). We therefore regard this to be a reasonable errorbar on each of our correlation results. If we simply take the mean of the 5 correlation values, we have 0.152, which is more than three standard deviations away from zero. We therefore regard the correlation to be significantly detected.

Let us consider the possibility that the Planck signal in the ($50 < l < 120$) modes is significantly polluted by noise and/or systematic effects. If the Planck map were all noise, how would one explain the correlation with BICEP2? But some noise contamination of the Planck $50 < l < 120$ map could help explain why its genus curve and histogram approximate the Gaussian random phase results as well as they do.

6.2 Calculations of the contributions of various components

Now we will analyze the situation in detail. We have

$$\sigma_B^2 = \sigma_{BGW}^2 + \sigma_{BN}^2 + \sigma_{BGL}^2 + \sigma_{BD}^2, \quad (6)$$

where σ_B is the standard deviation in the BICEP2 map, σ_{BGW} is the standard deviation of the BICEP2 gravity wave signal, σ_{BN} is the standard deviation of the BICEP2 noise, σ_{BGL} is the standard deviation of BICEP2 gravitational lensing signal, and σ_{BD} is the standard deviation of the BICEP2 dust signal (since all these are uncorrelated with each other, they add in quadrature to give σ_B^2 for the whole map). The BICEP2 team has produced a simulated map showing only the expected gravitational lensing and noise. From our digitization of this map, which includes only gravitational lensing and noise, we find its standard deviation to be $\sigma_{sim} = 0.0561\mu\text{K} = 0.670\sigma_B$ (somewhat higher than the approximate value of 0.5 that the BICEP2 team implied

in their figure. To be precise, they said that their map amplitude was more than twice the simulation amplitude at the $l = 70$ mode [we verified this]. That is in the middle of the range where the gravity waves are most prominent, so the overall ratio should be expected to be somewhat less, which is what our digitization shows.). The simulation has an amplitude

$$\sigma_{sim}^2 = \sigma_{BN}^2 + \sigma_{BGL}^2 = [0.0561\mu\text{K}]^2 = 0.448\sigma_B^2. \quad (7)$$

We now consider the correlation between the dust map and the BICEP2 map. In Fig. 14 we show the correlation by shading in red positive-positive correlations, in blue negative-negative correlations and in green negative-positive or positive-negative anti-correlations. One can see that the most significant features in the dust map (one major red spot and one major blue spot) are, in fact, correlated with the BICEP2 map. To calculate the correlation coefficient C_{PB} between the Planck and BICEP2 maps, we divide each map by its standard deviation, and then multiply the two maps and average over the pixels. The noise in the BICEP2 and the noise in the Planck are uncorrelated, and so their product averages to zero. The signal terms appear as products (e.g., $\sigma_{BGW}\sigma_{PGW} = \sigma_{BGW}^2$). The gravity wave and gravitational lensing signals should be equal in both maps. We will now write the formula for the Planck 353-BICEP2 correlation coefficient, C_{PB} :

$$C_{PB} = \frac{\sigma_{BGW}^2 + \sigma_{BGL}^2 + \sigma_{BD}\sigma_{353D}}{\sigma_B\sigma_{353}} \quad (8)$$

Since the noise in BICEP2 and noise in Planck are uncorrelated, and since $\sigma_{BGW} = \sigma_{PGW}$ and $\sigma_{BGL} = \sigma_{PGL}$, we know $\sigma_{BN}^2 + \sigma_{BGL}^2 = 0.448\sigma_B^2$, but not the specific value of σ_{BGL}^2 . So let's set $z = \sigma_{BGL}^2/\sigma_B^2$. Then $0 < z < 0.448$. Set $w = \sigma_N^2/\sigma_B^2$. Then $w + z = 0.448 = z_{max}$. From our calculation of the frequency effects on the dust signal, we have $\sigma_{353D} = 21.3\sigma_{BD}$. Substituting, we get

$$C_{PB}\sigma_{353} = \frac{\sigma_{BGW}^2 + \sigma_{BGL}^2 + 21.3\sigma_{BD}^2}{\sigma_B} \quad (9)$$

With $x = \sigma_{BGW}^2/\sigma_B^2$ and $y = \sigma_{BD}^2/\sigma_B^2$ we have

$$C_{PB}\sigma_{353}/\sigma_B = x + z + 21.3y \quad (10)$$

Referring to equation (6) and (7), we find

$$x + y = 1 - [(\sigma_{BN}^2 + \sigma_{BGL}^2)/\sigma_B^2] = 1 - 0.448 = 0.552 \quad (11)$$

We can estimate the value of z from Fig. 2 of the BICEP2 paper (BICEP2 2014a), which shows their measured power spectra, and theoretical contribution due to gravitational lensing. We know the noise power spectrum $C_l \sim \text{const}$, just as with the gravitational lensing power spectrum, and we can determine its amplitude from the stated value of 87nK in a square degree patch. Using HEALPix, we construct a $C_l \sim \text{const}$ map, and measure the rms amplitude in 1 square degree patches. We can measure the theoretical C_l for gravitational lensing at $l = 119$ from Fig. 2 in the BICEP2 paper (BICEP2 2014a). The theoretical C_l amplitude is of course based on lensing data from Planck and elsewhere. Taking the ratio of the C_l 's from lensing and noise at $l = 119$ allows us to calculate that the ratio $z/w = 0.774$. The noise and gravitational lensing power spectra are proportional to each other (both have $C_l \sim \text{const}$ over the range $50 < C_l < 120$), so we can get the ratio z/w from the ratios of the C_l 's at

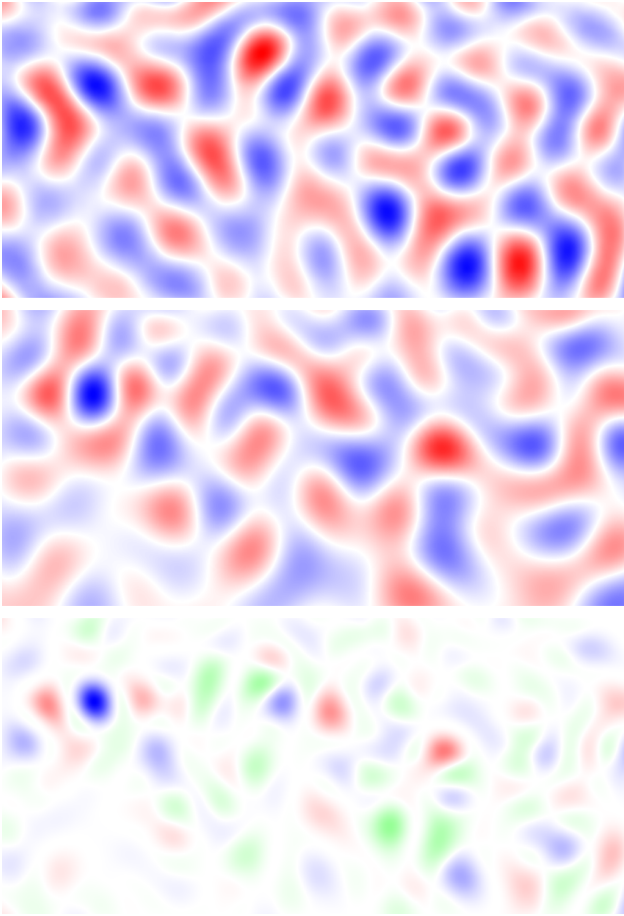


Figure 14. At top, the BICEP2 map (as in Fig. 1); in the middle, our Planck 353 GHz Map IV (as in Fig. 7). At bottom is the correlation of these two maps. All maps are in Mercator projection in the region $|\text{RA}| \leq 30^\circ$, $-65^\circ \leq \text{Dec} \leq -50^\circ$. Red shows positive-positive correlations; blue shows negative-negative correlations; green shows anti-correlations (negative-positive or positive-negative).

$l = 119$. We will therefore adopt $z/w = 0.774$. Then, using $w + z = 0.448$, we find $z = 0.1955$. We can now solve the two equations above for x and y . Substituting we find

$$C_{PB}(\sigma_{353}/\sigma_B) = 0.552 + 0.1955 + 20.3y \quad (12)$$

We can then solve for y and find $x = 0.552 - y$. The equation can also be rewritten as

$$C_{PB}(\sigma_{353}/\sigma_B) = 1 - w + 20.3y, \quad (13)$$

which we will find useful later. To estimate the tensor-to-scalar mode ratio r , we simply utilize the BICEP2 team's power spectrum calibration. In our notation, that is simply $r = (x/0.552) \cdot 0.2$. In other words, if there were no dust ($y = 0$), $x = 0.552$ and we would find $r = 0.2$, as calibrated by BICEP2's power spectrum analysis. We present in Table 1 those results for Planck Maps I – V.

The mean value of r from the 5 methods is $r = 0.106$. A simple estimate of the uncertainty associated with our values of r is the direct standard deviation of the above values from the different methods; that computes to ± 0.020 . This is a reasonable estimate of the error associated with our varied mapping processes. (For comparison, one could

Table 1. Relative contributions to BICEP map, for different analyses of the dust. The error on each measured correlation, C_{PB} , is estimated to be 0.039. C^* refers to the correlation necessary to imply a r of 0. In all cases, the correlation measured is at least 2.5σ below this level (for Maps I–V, these levels are 2.6σ , 4.9σ , 3.1σ , 4.1σ and 3.1σ).

| Map | $\sigma_{353}(\mu\text{K})$ | C_{PB} | C^* | x | y | r |
|---------|-----------------------------|----------|-------|-------|-------|-------|
| Map I | 4.97 | 0.101 | 0.202 | 0.292 | 0.259 | 0.106 |
| Map II | 3.31 | 0.112 | 0.302 | 0.370 | 0.181 | 0.134 |
| Map III | 3.12 | 0.202 | 0.321 | 0.219 | 0.333 | 0.079 |
| Map IV | 2.96 | 0.181 | 0.337 | 0.274 | 0.278 | 0.099 |
| Map V | 3.03 | 0.161 | 0.331 | 0.301 | 0.250 | 0.109 |

apply median statistics [c.f. Gott et al. 2001] to our 5 r values; the median value is $r = 0.106$, while the chance the true value is between 0.99 and 0.109 is 62.5%, roughly 1σ .) If we used the independent $\sigma_{353D} = 23.1\sigma_{BD}$ estimate from a simple power-law interpolation between Planck at 353 GHz and Planck at 143 GHz to estimate the dust amplitude at 150 GHz, we would have gotten a mean value of $r = 11.4$. Thus the uncertainty in r to due the uncertainty in this ratio is ± 0.008 . However, there is still some additional error in the estimate of z . The BICEP2 team reports that the gravitational lensing power can vary by about 45.5%. As such, we recomputed our x , y and r values with z increased and decreased by 45.5% (z_{max} was adjusted by the same resulting addends on z); this introduces an additional error of 0.016. Note that Equation (12) shows that adding or subtracting $(0.455 \times 0.1955) = 0.089$ from z changes y not at all, but adds or subtracts 0.089 from x with consequent changes of r of ± 0.016 . We also have the error in r introduced by the 0.039 error in the correlation measurements; this translates to an error of 0.029 in r . Each individual map has an uncertainty in its correlation coefficient C_{PB} of ± 0.039 determined as we have described, by cross-correlating BICEP2 with random Planck 353 fields. We raise and lower C_{PB} by this amount to compute the error bias on r in each of the 5 maps. The rms value of this 1σ error in r is 0.029. So, we take as our best value $r = 0.106$ (this is both the mean and the median of the values from our 5 maps). As our very conservative estimate of the error in r , we will add in quadrature the standard deviations of the r values from the 5 different maps, errors in the factor 21.3, the errors due to the expected errors in the correlation coefficients, and the errors due to the uncertainty in gravitational lensing: $r = 0.106 \pm 0.039$. Rounding and keeping significant digits, $r = 0.11 \pm 0.04$.

It is important to note that these varied methods give consistent results. Map I, for example, includes ringing in the $50 < l < 120$ modes from the Galactic plane. This ringing just adds noise, which boosts the value of σ_{353} and lowers the correlation by a factor of 1.7 relative to the lower noise Map IV, but both give similar values of r .

Furthermore, we can explore what value of the correlation would be necessary to drive the gravitational wave component, x to zero in our maps (see Table 1). For Map IV, we find that a correlation of 33.7% would be necessary. This value is more than 3σ outside our observed correlation of 0.181 ± 0.039 .

Of course, the σ value from the BICEP2 map is somewhat lower than one might naively expect from the power

spectra given by the BICEP2 team, due to despinning and limiting the spherical harmonic modes to $50 < l < 120$. We find for a pure noise map, for the Planck map, and for the BICEP2 map, the power spectra were all suppressed by an equivalent factor by all of this processing, which leaves the analysis of the ratios and correlations intact.

As an example, suppose the BICEP2 analysis drops ambiguous modes (to avoid leakage of E -modes into B -modes) and drops other modes for experimental reasons. Their calculation of the power spectrum will take these drop-outs into consideration, but the map might be missing these modes. Thus $\sigma_B^2 = \sigma_1^2 + \sigma_2^2$, where the map includes modes labeled 1 and excludes the modes labeled 2. The observed BICEP2 map will have an amplitude σ_1 , slightly lower than the amplitude it should have (σ_B). Assume the Planck map includes both modes labeled 1 and 2 and therefore has the expected amplitude σ_{353} . The amplitude of the gravity wave portion of the BICEP2 map is now $\sigma_{GW}(\sigma_1/\sigma_B)$, which correlates only with the (1) modes in the Planck Map which have an amplitude of $\sigma_{GW}(\sigma_1/\sigma_B)$, thus the product of the gravity wave modes in the two maps is: $\sigma_{GW}^2(\sigma_1/\sigma_B)^2$. We have similar terms for gravitational lensing modes and dust modes. In equation (8) the numerator on the right hand side is multiplied by a factor of $(\sigma_1/\sigma_B)^2$ while the denominator is multiplied by a factor of (σ_1/σ_B) . This multiplies C_{PB} by a factor of (σ_1/σ_B) . In equation 10 the left side of the equation $C_{PB}(\sigma_{353}/\sigma_B)$ is unchanged, because both C_{PB} and σ_B have been multiplied by a factor of (σ_1/σ_B) while σ_{353} remains as before; this leaves $x + z + 21.3y$ unchanged. Our solutions for x , z , and y remain unchanged as does our result for r . Thus, our results are not affected if the BICEP2 map drops some some modes.

The Planck team and the BICEP2 team have agreed to a joint analysis of their data. The BICEP2 team can “observe” the Planck 353 map using their procedures which would involve dropping just the (2) modes. Thus, their final “Planck map” would have an amplitude of $\sigma'_{353} = \sigma_{353}(\sigma_1/\sigma)$ because the BICEP2 analyzed Planck map contains only the (1) modes. The BICEP2 team would then find a correlation coefficient between their current map with amplitude σ_1 and the new “Planck Map” with amplitude of σ'_{353} of $C'_{PB} = (x\sigma_1^2 + z\sigma_1^2 + 21.3y\sigma_1^2)/(\sigma_1\sigma'_{353})$, giving $C'_{PB}\sigma_{353}'/\sigma_1 = x + z + 21.3y$. The BICEP2 team will observe a correlation coefficient C'_{PB} with their new reduced “Planck Map” that is higher than we observe by a factor of σ_B/σ_1 , but this is compensated for exactly by the fact that σ'_{353} is smaller than what we observe by the same factor, so that they should get the same value of $x + z + 21.3y$ that we get. In the same way, we showed in our comparison with Map I, that addition of ringing modes from outside the BICEP2 region to the Planck map, by raising the amplitude of σ_{353} while simultaneously lowering the correlation coefficient by the same factor leads to a similar estimated value of $r = 0.106$. Planck (Planck Collaboration 2014b) has (since our original preprint was published on arXiv) produced an apodized map of the BICEP2 region which is similar in construction to our Map IV. They have not published this map, but have used it to make power spectrum amplitude estimates of the B and E -modes (from $40 < l < 120$). The ratio of their E and B -mode powers in their map is equal to what we get from our digitized Map IV to within 1σ . We observe a correlation coefficient of $C_{PB} = 0.181$ between the

BICEP2 map and our Map IV at 353 GHz. We obtained a value of $r = 0.099$ with Map IV. The Planck team simultaneously, upped their best estimate for the ratio of the dust signal amplitude ratio $\sigma_{353D}/\sigma_{BD}$ to 24.5. This is higher than our adopted value of 21.3 and this has the effect of slightly raising the value of r . Applying both Map IV and the value of 24.5 leads to a best estimate of $r = 0.104$. The errors would be similar to our earlier estimates. Rounding as we did before and keeping significant figures would give us $r = 0.10 \pm 0.04$, compared with our original estimate of $r = 0.11 \pm 0.04$. The difference is insignificant within the errors. Our error budget already included errors for the factor of 21.3, and for the errors associated with picking different maps for comparison.

The power spectrum of the lowest polarization 30% of the sky in Planck at 353 GHz seems to hit noise at $C_l \sim 2.2 \times 10^{-3} \mu K^2$ at $l \sim 260$, where one is looking at noise amplitudes of $\Delta_{BB}^2 \sim l(l+1)C_l/4\pi \sim 11.5 \mu K^2$. This noise estimate in the B -modes is empirically based on when measurements of the B -modes by Planck start to show uncertainty. This very rough estimate from the Planck power spectrum suggests $\sigma_{353N} \sim 3.4 \mu K$, similar to σ_{353} , suggesting noise makes a significant contribution to the Planck map. The Planck team notes that to look for a gravity wave signal at $r = 0.1$ will require subtraction of the dust signal. This means correlating the two maps. The fact that we observe a significant but low correlation with BICEP2 allows us to quantify the contribution of the dust signal. Assuming σ_{353} was entirely due to dust (with no noise) would lead to an overestimate of the dust contribution to the BICEP2 map. Assuming that the excess B -modes in the BICEP2 were due entirely to dust (and not at all to gravity waves) would have produced correlations larger than we observed. Our correlation study allows us to quantify the dust contribution to the BICEP2 signal, and we find it to be slightly less than the gravity wave signal.

In conclusion our independent analysis shows evidence supporting a detection of a gravity wave signal with $r = 0.11 \pm 0.04 (1\sigma)$. The Planck team and the BICEP2 team have agreed to a joint analysis of their data. It will be interesting to see if they reach similar conclusions. We look forward to that paper.

ACKNOWLEDGEMENTS

We thank Joel Zinn, Bruce Draine, Lyman Page, Matias Zaldarriaga and David Spergel for helpful conversations.

REFERENCES

- BICEP2 Collaboration, 2014a, arXiv:1403.3895 [astro-ph.CO]
- BICEP2 Collaboration, 2014b, http://bicepkeck.org/B2_2014_i_figs/eb_maps.pdf
- BICEP2 Collaboration, 2014c, arXiv:1403.4302 [astro-ph.CO]
- Boulanger, F., 2014, <http://www.rssd.esa.int/SA/PLANCK/docs/eslab47/S>
- Coles, P., & Plionis, M., 1991, MNRAS, 250, 75
- Colley, W.N., 1997, ApJ, 489, 471

- Colley, W.N., 1998, PhD Thesis, Princeton Univ., Princeton, NJ
- Colley, W. N. & Gott, J. R. 2003, MNRAS, 344, 686
- Colley, W. N., Gott, J. R. & Park, C. B., 1996, MNRAS, 281: L82
- Draine, B. T. & Hensley, B., 2013, ApJ, 765: 159
- Flauger, R., Hill, J. C. & Spergel, D. N. Spergel, 2014, arXiv:1405.7351v1 [astro-ph.CO]
- Górski, K.M., Hivon, E., Banday, A.J., Wandelt, B.D., Hansen, F.K., Reinecke, M. & Bartelmann, M., 2005, ApJ, 622, 759
- Gott, J. R., Choi, Y-Y., Park, C. & Kim, J. 2009, ApJ, 695: L45
- Gott, J. R., Colley, W. N., Park, C-G., Park, C., & Mugnolo, C., 2007, MNRAS, 377, 1668a
- Gott, J. R., et al., 1989 ApJ, 340: 625
- Gott, J. R., Park, C., Juszkiewicz, R., Bies, W. E., Bennett, D. P., Bouchet, F. R. & Stebbins, A., 1990, ApJ, 352, 1
- Gott, J. R., Melott, A., Dickinson, M., 1986, ApJ, 306, 341
- Gott, J.R. & Slepian, Z., 2011, MNRAS, 416, 907
- Gott, J. R., Vogeley, M. S., Podariu, S. & Ratra, B., 2001, ApJ 549:1
- Gott, J. R., Weinberg, D., Melott, A., 1987, ApJ, 319, 1
- Guzik, J., Seljak, U. & Zaldarriaga, M., 2000, Phys. Rev. D, 62, 043517
- Hamilton, A. J. S., Gott, J.R. & Weinberg, D. H., 1986, ApJ, 309, 1
- Hivon, 2010, map2alm.spin* documentation, <http://healpix.jpl.nasa.gov/html/subroutinesnode47.htm>
- Kamionkowski, M., Kosowsky, A. & Stebbins, A., 1997, Phys. Rev. Lett., 78, 2058
- Kamionkowski, M. & Kovetz, E.D., 2014, arXiv:1408.2125 [astro-ph.CO]
- Melott, A., Cohen, A.P., Hamilton, A. J. S., Gott, J. R. & Weinberg, D. H., 1989, ApJ, 345, 618
- Mortonson, M. J. & Seljak, U., 2014, arXiv:1405.5857v1 [astro-ph.CO]
- Opperman, N. et al., 2011, arXiv: 1111.6186v2 [astro-ph.GA]
- Park, C. & Kim, Y-R., 2010, ApJL, 715, 185
- Planck Collaboration, 2013, arXiv:1303.5084 [astro-ph.CO]
- Planck Collaboration, 2014a, arXiv:1405.0874 [astro-ph.CO]
- Planck Collaboration, 2014b, arXiv:1409.5738 [astro-ph.CO]
- Seljak, U. & Zaldarriaga, M., 1997, Phys. Rev. Lett. 78, 2054
- Slepian, Z., Gott, J.R. & Zinn, J., 2014, MNRAS, 438, 1948
- Spergel, D.N., Bean, R., Doré, O., Nolta, M.R., Bennett, C.L., Hinshaw, G., Jarosik, N., Komatsu, E., Page, L., Peiris, H.V., Verde, L., Barnes, Halpern, C.M., Hill, R.S., Kogut, A., Limon, M., Meyer, S.S., Odegard, N., Tucker, G.S., Weiland, J.L., Wollack, E., & Wright, E.L., 2007, ApJSS, 170, 377